ChemComm

COMMUNICATION

View Article Online
View Journal

Cite this: DOI: 10.1039/c9cc08457f

Received 29th October 2019,
Accepted 27th January 2020

DOI: 10.1039/c9cc08457f

rsc.li/chemcomm

Aggregation induced emission (AIE) active 4-amino-1,8-naphthalimide-Tröger's base for the selective sensing of chemical explosives in competitive aqueous media†

Jason M. Delente,[ab] Deivasigamani Umadevi,[c] Sankarasekaran Shanmugaraju,*[d] Oxana Kotova,[a] Graeme W. Watson[c] and Thorfinnur Gunnlaugsson*[ab]

The 4-amino-1,8-naphthalimide-Tröger's base fluorophore, TBNap-TPy, adorned with phenyl-terpyridine moiety was synthesised and assessed for its aggregation-induced emission (AIE) behaviour. TBNap-TPy was further employed as a fluorescent sensor for the discriminative sensing of π-electron-deficient nitroaromatic; the TBNap-TPy displaying the largest fluorescence quenching with high selectivity for picric acid, a harmful environmental pollutant widely used in the dye industries.

Supramolecular chemistry has been used to form dynamic and intricate structures and materials demonstrating various properties ranging from gelators,[1] bioimaging agents,[2] and luminescent sensors,[3] to name a few. Fluorescence 'on–off' and 'off–on' switching systems are highly attractive chemosensors due to their simplicity of uses, high sensitivity and fast response time.[3] Recently, the phenomenon of aggregation-induced emission (AIE) and aggregation-induced emission enhancement (AIEE), has been developed for use in chemical sensing and bio-imaging.[4] Unlike many fluorophores, which often suffer from aggregation-caused quenching (ACQ), the common strategy for designing AIE or AIEE fluorophores is to functionalise the fluorophore with bulky substituents or a long branched chains with the aim of restraining intramolecular rotation, which will lead to the loss of excited energy only through radiative pathway.[5] Many examples of fluorophores have been shown to achieve AIE/AIEE sensors such as pentacenequinone,[6] tetraphenylethene,[7] anthracene,[8] hexaphenylsiloles.[9] Naphthalimide (**Nap**) based fluorescence sensors have attracted substantial attention in fluorescence sensing,[10] and have recently been shown to be candidates for use in AIE based systems.[2,3] Poly-nitroaromatic compounds (NACs) are secondary chemical explosives and are used widely as pigments in various dye and textile industries.[11–13] While several examples of fluorescent sensors for NACs exists, there currently exist the need to develop a suitable and reliable fluorescence sensor for the trace detection of NACs in competitive media.[12,13] By taking advantage of the AIE design, luminescent sensors have recently been developed that are able to compete with the metal–organic framework (MOF) and coordination polymers for sensing of NACs.[13] These AIE examples have shown both good sensibility and selectivity, as well as enabling such sensing in more competitive aqueous media.[6,11,14] Recently, using 4-amino-1,8-naphthalimide Tröger's base motifs (**TBNaps**), we have developed a variety of materials for the discriminative detection of NACs such as picric acid (PA), including organic polymers and coordination networks.[13,15] We have shown that these structures are able to sense PA with both high sensitivity and selectivity where the sensing action was monitored through observing the luminescent 'on–off' and 'off–on' switching properties in water.

The **Nap** derived **TBNaps** are novel and highly versatile supramolecular building blocks that we have been developing over the last decade.[2,13,16] Due to the almost orthogonal orientation between the two **Nap** fluorophores [caused by the chiral cleft-shaped diazocine ring (Tröger's bases) unit] in **TBNaps**, we have shown, through the use of solid-state crystallography, that the **TBNaps** can give rise to variety of solid-state stacking interactions; the nature of which is dictated by (a) the structural unit incorporated at the imide site and (b) the solvent media. With the aim of capitalising on this aggregation property of the **TBNaps** we set out to (i) develop the first examples of AIE based **TBNaps**, and (ii) demonstrate their applications in fluorescence AIE sensing. Herein, we present our result into the use of **TBNap-TPy**, the phenyl-terpyridine, and 4-amino-1,8-naphthalimide based

[a] School of Chemistry and Trinity Biomedical Sciences Institute, Trinity College Dublin, The University of Dublin, Dublin 2, Ireland. E-mail: gunnlaut@tcd.ie
[b] AMBER (Advanced Materials and Bioengineering Research) Centre, Trinity College Dublin, The University of Dublin, Dublin 2, Ireland
[c] School of Chemistry and Centre for Research on Adaptive Nanostructures and Nanodevices (CRANN), Trinity College Dublin, The University of Dublin, Dublin-2, Ireland
[d] Chemistry, Indian Institute of Technology Palakkad (IITPKD), Kerala, India. E-mail: shanmugam@iitpkd.ac.in

† Electronic supplementary information (ESI) available: Experimental details, synthesis and characterisations details (multinuclear NMR, IR, HRMS), fluorescence studies and computational calculations. See DOI: 10.1039/c9cc08457f

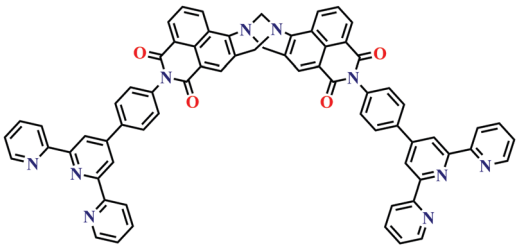

Fig. 1 Structure of **TBNap-TPy** fluorophore studied herein.

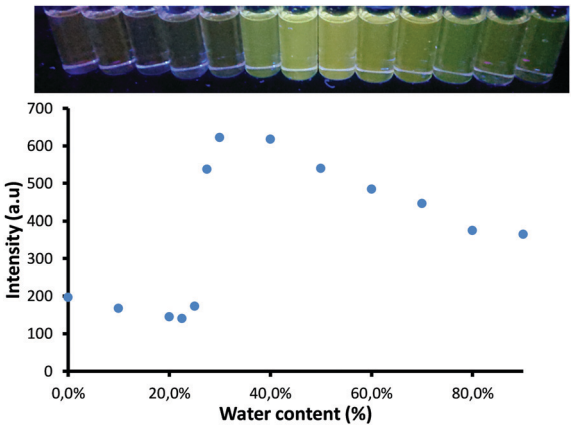

Fig. 2 Intensity plot of **TBNap-TPy** (c = 4.6 × 10^{-6} M) in DMSO upon addition of water. Inset: Visible colour changes observed under UV lamp (ex. 360 nm).

Tröger's base, as an AIE based sensor for NACs. During the design of **TBNap-TPy**, we anticipated that by incorporating phenyl-terpyridine (TPy) moieties, being π-electron-rich, into the **TBNap** framework (*e.g.* Fig. 1) would: (i) enhance the sensing propensity of the **TBNap** towards π-electron-deficient NAC,[15] and (ii) in counter-solvents, lead to hindering in the molecular free-rotation of the TPy rings, which would enable AIE.

The **TBNap-TPy** was synthesised from the commercially available acetylpyridine, 4-nitrobenzaldehyde, and 4-nitro-1,8-naphthalic anhydride, in few steps. Formation of 4′-(4-nitrophenyl)-2,2′:6′,2″-terpyridine was achieved following the procedure described by Brudvig *et al.*[17] while the formation of the desired Tröger's base **TBNap-TPy** was carried out using methods developed in our laboratory (see full details in ESI†).[15,16] The successful formation of **TBNap-TPy** was demonstrated by HRMS and elemental analysis (see ESI†). The ^{1}H NMR in DMSO-d_6 confirmed the formation of the Tröger's base moiety with the presence of the two well-defined doublets at 5.23 and 4.74 ppm corresponding to the methylene protons of the diazocine ring (see ESI†).[16] The IR spectrum of **TBNap-TPy** reveals two peaks at 1705 cm^{-1} and 1665 cm^{-1} accounting for the carbonyl groups on the naphthalimide moieties and a strong signal at 1240 cm^{-1} due to C–N stretching of the Tröger's base unit.[13]

The luminescence behaviour of **TBNap-TPy** in solution was studied with the use of various organic solvents and mixtures of organic-aqueous solutions. In general, the results demonstrated the presence of a red shift of the emission spectrum upon increasing polarity which is an indicator of the presence of internal charge transfer (ICT) state due to the push–pull nature of the donating amine and the withdrawing imide. This is typical for amino-**Naps** and we demonstrated the same for the **TBNaps**, though the diazocine ring reduces the strength of the push–pull interactions leading to a small blue shift in the **TBNap** emission *vs.* the **Nap** emission (see ESI†).[16] The discussion below will, due to the nature of the work, focuses on these properties in DMSO and mixed DMSO–H_2O solutions. The electronic absorption spectra of the ligands in DMSO (see ESI†) was dominated by ligand-centred π → π* transitions centred at 278 nm (ε = 98 919 ± 388 cm^{-1} M^{-1}), 319 nm (ε = 27 929 ± 146 cm^{-1} M^{-1}), 346 nm (ε = 18 864 ± 142 cm^{-1} M^{-1}), and the ICT Tröger's base band centred at 388 nm (ε = 21 303 ± 134 cm^{-1} M^{-1}).[16,18] As we had anticipated, then upon adding deionized H_2O to the DMSO solutions, an enhancement in the fluorescence was observed, due to enhanced aggregation of **TBNap-TPy** and the 'switching on' effect of the AIE; the effect is clearly visible even to the naked eye as demonstrated in Fig. 2. We studied this effect further by measuring the changes in the absorbance, fluorescence and excitation spectrum of **TBNap-TPy** (c = 4.6 × 10^{-6} M) at the various percentage of H_2O in DMSO (see full details in ESI†). All the work was carried out in triplicates and found to be fully reproducible. In the absorbance spectrum, no significant changes were observed in the ground state upon the addition of H_2O compared to that seen in DMSO. In contrast, the fluorescence excitation spectrum exhibited a significant shift from 450 nm to 400 nm for the ICT transition when the H_2O content was changed from 20 → 40%.[19] These changes reflecting the **TBNap-TPy** aggregation in the more polar protic solution. Upon excitation of the ICT band in DMSO, broad fluorescence emission was observed with λ_{max} at 530 nm. Upon the addition of H_2O, no significant shifts were seen in the λ_{max}. However, a significant 3-fold enhancement was observed in the emission intensity (see ESI† and Fig. 2.), with maximum intensity being observed at 30% H_2O. Once the water content increased beyond this, the emission intensity slowly decreased, stabilising between 80–90% of H_2O as demonstrated in Fig. 2. To gain further insight into the aggregation effects and their associated morphological features, we employed FE-SEM to probe the aggregate formation at various DMSO:H_2O fractions. As can be seen in Fig. 3, the FE-SEM analysis demonstrates the formation of amorphous aggregates with the presence of a random distribution of spherical particles. As the water content increased, the number of spherical aggregates increased, becoming the predominant structural feature when the water content reaches 30%. The spherical aggregates have a size ranging from 48 nm to 300 nm. Upon increasing the water content above 30% the spherical aggregates are destroyed, forming amorphous aggregates that demonstrate the influence of the solvent on the self-assembly of **TBNap-TPy**.[1]

Having established the optimum emission properties for **TBNap-TPy** in the H_2O–DMSO mixture, we next investigated the potential application of this system as a luminescent sensor for pollutants in water, such as PA, which was used as a prototype of NACs, where the changes in the ICT emission of **TBNap-TPy** were monitored. PA is extensively used in industry, and is considered as environmental pollutants and potentially toxic to living organisms.[12,13] It has a high solubility in water (~14 g L^{-1}), and as such is stored and transported in water across the world.[15] The continuous exposure to saturated

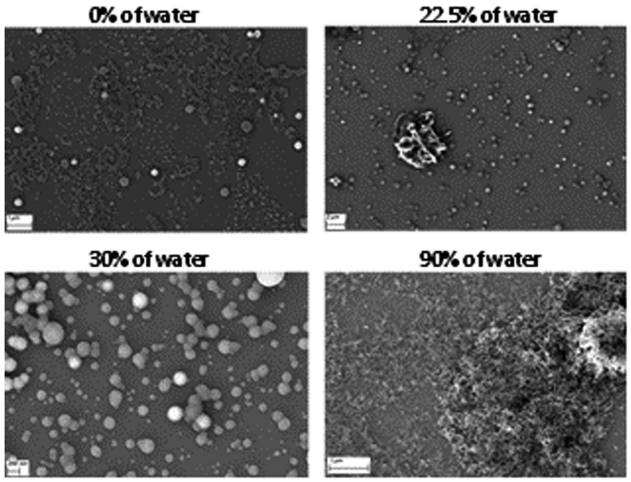

Fig. 3 Scanning electron microscopy images of **TBNap-TPy** at various percentage content of water in DMSO.

vapours of PA can cause severe and un-repairable health issues like liver and kidney failure and neurological damages and as such it is a highly desirable target for chemosensing in competitive media.[11,13–15] The changes in the ICT centered emission of **TBNap-TPy** upon increasing concentration of PA are shown in Fig. 4. As can be seen, no significant changes in λ_{max} were observed, while significant quenching in the **TBNap** fluorescence was observed between 0–74.1 μM of PA. The observed significant fluorescence quenching clearly indicates a strong interaction between PA and aggregated state of **TBNap-TPy**. The quenching propensity was thus next analyzed using the Stern–Volmer equation. The results are shown as an inset in Fig. 4, showing a slight upward curvature upon increasing PA concentrations, which could indicate that both static and dynamic quenching occurred.[13a] Nevertheless, the linear region of these changes was fitted to a Stern–Volmer plot and gave $K_{sv} = 4.06 \pm 0.4 \times 10^4\ M^{-1}$, which is comparable to what has been observed for similar systems.[13a]

Density functional theory (DFT) analysis was performed using the M06-2X/6-311G(d,p)[20] method to understand the interactions between **TBNap-TPy** and PA using the model system (see ESI†). All the calculations were done by using Gaussian 09 package.[21] The frontier molecular orbital calculations show that the HOMO is more localized in the Troger's base and naphthalene region while the LUMO is more localized in the imide region of **TBNap** (ESI†). This confirms that **TBNap** moiety is electron-rich. The structure of

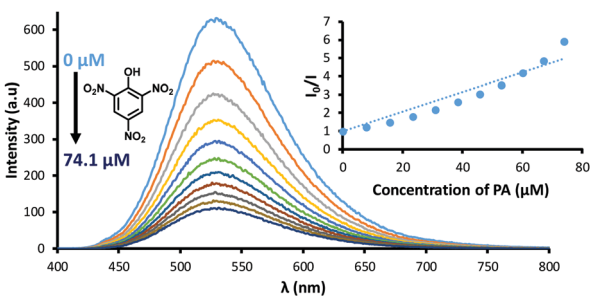

Fig. 4 Fluorescence quenching of **TBNap-TPy** upon addition of PA. Inset: The corresponding Stern–Volmer plot for the quenching.

TBNap-TPy indicates five possible sites ($-N_{Tröger's}$, $-C{=}O_{imide}$, $-N_{imide}$, $-N_{Py1}$, $-N_{Py2}$) where **TBNap-TPy** could interact with PA (ESI†). Our calculations showed that PA exhibits intermolecular interactions at $-N_{Tröger's}$, $-C{=}O_{imide}$, $-N_{Py1}$, and $-N_{Py2}$ sites with binding energies 8.45, 15.90, 23.87 and 18.46 kcal mol^{-1}, respectively. The optimized geometries indicate hydrogen-bond interactions at the $-N_{Tröger's}$, and $-N_{Py1}$ sites and a combination of hydrogen-bonding and π–π stacking type of interactions at the $-C{=}O_{imide}$, $-N_{Py1}$ sites (ESI†). No such stable interaction was observed at the $-N_{imide}$ site. The higher binding energies observed at the TPy moieties are in good agreement with the observed enhanced sensing propensity of **TBNap** adorned with TPy moieties. To substantiate this experimentally, a ^1H NMR titration study between **TBNap-TPy** and PA was carried out, which shows a significant downfield shift for proton resonances of TPy moiety upon the gradual addition of PA, while the proton resonance of **TBNap** showed no to little changes (ESI†). This substantiates our assumption that TPy moiety forms strong π-stacking interactions with PA. We further analyzed the FT-IR spectra of PA and **TBNap-TPy** before and after mixing with PA (ESI†). In the FTIR spectrum of PA after mixing with **TBNap-TPy**, the peak corresponding to the –OH stretching of PA was completely disappeared confirming the existence of strong intermolecular hydrogen-bonding interactions between **TBNap-TPy** and PA.[15]

To demonstrate the mechanism of fluorescence quenching, the time-resolved fluorescence decay at different concentrations of PA was recorded, and the temperature dependence quenching in the **TBNap-TPy** emission in the presence of PA was analyzed. Both the time-resolved decay of **TBNap-TPy** in DMSO and in the 70 : 30 DMSO–H_2O mixture were fitted to bi-exponential decay, which showed that upon addition of PA, the excited state lifetimes were decreasing respectively from 2.52 ns to 1.85 ns for τ_1, and 7.44 ns to 6.20 ns for τ_2; this revealing the interaction of PA to **TBNap-TPy** in the excited state (see ESI†).[13a] These measurements were shown to be fully reproducible. The temperature dependence experiment in presence of 38.5 μM of PA also revealed that the quenching efficiency was 59% at 24.5 °C, being dramatically increased to 70% at 45 °C (ESI†). This can be accounted by two phenomena; (i) enhancement in dynamic quenching upon raising the temperature, due to enhanced rate of collision between **TBNap-TPy** and PA, and (ii) to the potential destruction of the **TBNap-TPy** emissive aggregates.[5,13a] We also found that the extent of fluorescence quenching was highly dependents on the solution pH (ESI†). In acidic pH = 2.4, the quenching efficiency was high ($K_{SV} = 11.3 \times 10^4\ M^{-1}$), but in basic medium (pH = 11) the efficiency was decreased considerably ($K_{SV} = 2.1 \times 10^4\ M^{-1}$) likely due to the lack of intermolecular hydrogen-bonding interactions at alkaline pH.[15]

In order to be used as an AIE sensor for PA in aqueous media, it was necessary to demonstrate that **TBNap-TPy** possessed a good selectivity and sensitivity. The selectivity of **TBNap-TPy** was evaluated by carrying out fluorescence titrations separately using other NACs such as 2,4-DNP, 2-NP, 3-NP, 4-NP, TNT, 2,4-DNT, 2,6-DNT, 2-NT, 3-NT, 4-NT and NB and determining their corresponding Stern–Volmer constant (see ESI†). These titrations revealed that highest quenching efficiency was indeed obtained

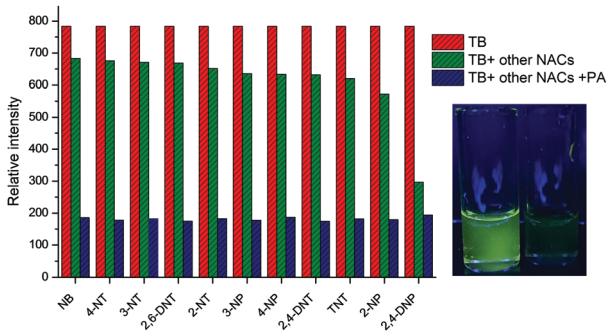

Fig. 5 Competitive selective affinity of **TBNap-TPy** ($c = 4.6 \times 10^{-6}$ M) towards different nitroaromatics in the presence of PA (74.1 μM) in DMSO–H_2O (70–30%) mixture. Inset: Visible colour changes observed before (left) and after (right) addition of PA (74.1 μM).

for PA with 83% (at endpoint) quenching in the AIE intensity; this being followed by 2,4-DNP which gave rise to 66% quenching at the same concentration. Furthermore, the analysis of these changes using the Stern–Volmer equation showed linear regression from which K_{sv} was determined (see details in ESI†). From this screening, it can be deduced that the phenolic-nitroaromatics (PA, 2,4-DNP, 2-NP, 3-NP, 4-NP) exhibited the highest quenching efficacy, which can be explained by the phenol group being able to form stronger intermolecular interactions with the Lewis basic nitrogen of the terpyridine and Tröger's base motifs.[13,15] The selectivity of **TBNap-TPy** towards phenolic nitroaromatics, and more specifically PA was further confirmed by performing competitive fluorescence studies, where a concentration of 74.1 μM of each of the NACs was added to a solution of **TBNap-TPy** (green bar, Fig. 5). This was followed by the addition of 74.1 μM of PA. The results (shown as blue bars in Fig. 5) clearly showed that in all cases to the **TBNap-TPy** emission was further quenched upon the addition of PA; which confirmed the high selectivity of **TBNap-TPy** towards PA. Furthermore, **TBNap-TPy** also displayed a strong binding affinity for PA in presence of various common ions except for a few transition metal cations such as Ni^{2+}, Co^{2+}, Cu^{2+} and Fe^{2+} showed a significant fluorescence quenching likely due to the metal–ligand chelation effect (see ESI†).[1] Gratifyingly, the PA quenching could also be seen with the naked eye under a UV lamp irradiation as demonstrated as an insert in Fig. 5. A sensitivity experiment was also carried out. The results (see ESI†) showed that the **TBNap-TPy** AIE response could be affected by PA even at 20 ppb concentration. Moreover, this level of sensitivity is under the allowed limit of NACs in drinking water established by the US EPA.[13,15] The response time towards PA was also evaluated at different PA concentrations; the results showing that upon addition of PA, the emission changes had equilibrated within a minute (see ESI†); the response time being independent of the concentration of PA employed. These overall results demonstrate that **TBNap-TPy** could potentially be used as a fluorescent AIE sensor for the on-site detection of PA.

In summary, we have synthesized **TBNap-TPy**, a 4-amino-1,8-naphthalimide Tröger's base functionalized with phenyl-terpyridine. We have shown the ability of this system to give rise to AIE in aqueous DMSO mixture. Taking advantage of this property we further demonstrated the fluorescent sensing of various NACs, where the selective sensing of PA and 2,4-DNP was demonstrated; the detection of PA being particularly selective.

We thank the Irish Research Council (IRC) for a postdoctoral fellowship (GOIPD/2015/290 to DU), Science Foundation Ireland (SFI PI Award 13/IA/1865 to TG) and the AMBER Centre for financial support, and Advanced Microscopy Laboratory-CRANN for the SEM analysis. All computation calculations were performed using the Lonsdale super computers-Trinity Centre for High-Performance Computing.

Conflicts of interest

There are no conflicts to declare.

Notes and references

1 A. J. Savyasachi, O. Kotova, S. Shanmugaraju, S. J. Bradberry, G. M. Ó'Máille and T. Gunnlaugsson, *Chem*, 2017, **3**, 764.
2 S. Erbas-Cakmak, S. Kolemen, A. C. Sedgwick, T. Gunnlaugsson, T. D. James, J. Yoon and E. U. Akkaya, *Chem. Soc. Rev.*, 2018, **47**, 2228.
3 P. Gopikrishna, N. Meher and P. K. Iyer, *ACS Appl. Mater. Interfaces*, 2018, **10**, 12081.
4 Z. He., C. Ke and B. Z. Tang, *ACS Omega*, 2018, **3**, 3267–3277.
5 J. H. Q. L. Z. Li, *Aggregation-Induced Emission: Fundamentals and Applications, vol. 1–2*, 2013, pp. 127–153.
6 S. Kaur, A. Gupta, V. Bhalla and M. Kumar, *J. Mater. Chem. C*, 2014, **2**, 7356.
7 Y. Dong, J. W. Y. Lam, A. Qin, J. Liu, Z. Li, B. Z. Tang, J. Sun and H. S. Kwok, *Appl. Phys. Lett.*, 2007, **91**, 011111.
8 H. Lu, B. Xu, Y. Dong, F. Chen, Y. Li, Z. Li, J. He, H. Li and W. Tian, *Langmuir*, 2010, **26**, 6838.
9 G. He, H. Peng, T. Liu, M. Yang, Y. Zhang and Y. Fang, *J. Mater. Chem.*, 2009, **19**, 7347.
10 R. Puglisi, A. Pappalardo, A. Gulino and G. Trusso Sfrazzetto, *ACS Omega*, 2019, **4**, 7550.
11 (*a*) N. Meher and P. K. Iyer, *Nanoscale*, 2017, **9**, 7674; (*b*) X. Cao, N. Zhao, H. Lv, Q. Ding, A. Gao, Q. Jing and T. Yi, *Langmuir*, 2017, **33**, 7788.
12 (*a*) S. Shanmugaraju, S. A. Joshi and P. S. Mukherjee, *J. Mater. Chem.*, 2011, **21**, 9130; (*b*) S. K. Kim, J. M. Lim, T. Pradhan, H. S. Jung, V. M. Lynch, J. S. Kim, D. Kim and J. L. Sessler, *J. Am. Chem. Soc.*, 2014, **136**, 495.
13 (*a*) S. Shanmugaraju, C. Dabadie, K. Byrne, A. J. Savyasachi, D. Umadevi, W. Schmitt, J. A. Kitchen and T. Gunnlaugsson, *Chem. Sci.*, 2017, **8**, 1535; (*b*) S. S. Nagarkar, B. Joarder, A. K. Chaudhari, S. Mukherjee and S. K. Ghosh, *Angew. Chem., Int. Ed.*, 2013, **52**, 2881.
14 Q. Lin, X.-W. Guan, Y.-Q. Fan, J. Wang, L. Liu, J. Liu, H. Yao, Y.-M. Zhang and T.-B. Wei, *New J. Chem.*, 2019, **43**, 2030.
15 S. Shanmugaraju, D. Umadevi, A. J. Savyasachi, K. Byrne, M. Ruether, W. Schmitt, G. W. Watson and T. Gunnlaugsson, *J. Mater. Chem. A*, 2017, **5**, 25014.
16 (*a*) S. Shanmugaraju, C. S. Hawes, A. J. Savyasachi, S. Blasco, J. A. Kitchen and T. Gunnlaugsson, *Chem. Commun.*, 2017, **53**, 12512; (*b*) E. B. Veale and T. Gunnlaugsson, *J. Org. Chem.*, 2010, **75**, 5513.
17 A. C. Durrell, G. Li, M. Koepf, K. J. Young, C. F. A. Negre, L. J. Allen, W. R. McNamara, H. E. Song, V. S. Batista, R. H. Crabtree and G. W. Brudvig, *J. Catal.*, 2014, **310**, 37.
18 P. Song, S.-g. Sun, P.-w. Zhou, J.-y. Liu, Y.-q. Xu and X.-j. Peng, *Chin. J. Chem. Phys.*, 2010, **23**, 558.
19 R. M. Duke and T. Gunnlaugsson, *Tetrahedron Lett.*, 2011, **52**, 1503.
20 Y. Zhao and D. G. Truhlar, *Theor. Chem. Acc.*, 2008, **120**, 215.
21 M. J. Frisch, *et al.*, *Gaussian 09*, Gaussian Inc., Wallingford, CT, 2009, see the ESI† for full citation.